Rapid 3D-Plastronics prototyping by selective metallization of 3D printed parts

Tony Gerges, Vincent Semet, Philippe Lombard, Bruno Allard, Michel Cabrera

Rapid 3D-Plastronics prototyping by selective metallization of 3D printed parts

Tony Gerges*, Vincent Semet, Philippe Lombard, Bruno Allard, Michel Cabrera

Univ Lyon, INSA Lyon, Université Claude Bernard Lyon 1, Ecole Centrale de Lyon, CNRS, Ampère, UMR 5005, 69621 Villeurbanne, France

***Corresponding author:** tony.gerges@insa-lyon.fr (T. Gerges)

Abstract

Nowadays, wide progress is being made in the technology field of selective metallization of polymer surface, in order to manufacture compact and miniaturized electronic devices. However, most of the developed methods are expensive, require sophisticated processes and in some cases involve the use of products that are toxic for health and environment. In this study, a new process being referred to as "Rapid 3D-Plastronics" was developed, combining 3D printing and 3D plastronics, a technology allowing integration of electronic circuits on 3D polymer parts by selective metallization. The originality of this work lies in combining easy, rapid and low-cost methods and limiting hazardous effects. The stereolithography (SLA) was used to produce the 3D parts and electroless plating to metallize the electronic circuitry. The tracks for the electronic circuit were defined and implemented in the design of the 3D printed part. The metal-polymer interface adhesion strength was enhanced using sandblasting and the surface morphology and contact angle were investigated. The selectivity of the electroless plating was guaranteed by localizing a palladium-based catalyst into the implemented tracks. The high electrical conductivity of the circuitry and the high adhesion of copper (Cu) circuitry obtained with this process were suitable for a sustainable operation of an electronic device. Operating rigid and flexible prototypes were manufactured and characterized to illustrate the potential application of the process. The Rapid 3D-Plastronics process proves satisfying for manufacturing complex 3D electronic devices, intended for use as heaters and sensors, high performance coil for Wireless Power Transfer, or flexible electronic circuits.

Keywords: 3D Plastronics, Additive manufacturing, Stereolithography, Rapid prototyping, Electroless plating, Flexible electronics.

1. Introduction

The 3D printing technology has expanded rapidly over the last years thanks to its attractivity in customization, prototyping and its ability to produce complex 3D geometries [1]. This advanced technique has the advantage of allowing design flexibility in the fabrication of 3D functional prototypes quickly, easily and at low cost. It has inspired many researchers to create customized devices with heterogeneous functions [2] and develop new processes intended for high performance polymers [3] and biodegradable polymers [4].

Among the different methods of 3D polymer printing, the stereolithography (SLA) process has the advantage of high printing accuracy, high temperature resistance and smooth surface finish [1,5]. SLA is a widely used technique for the fabrication of prototypes. A movable UV source is used to activate the polymerization of a photocurable resin and to build parts layers by layers from a computer aided design (CAD) file. SLA usually uses 405 nm waveband laser, and a methacrylate-based photo-polymerizable resin [6]. Such photocurable resins are used in many other fields thanks to their chemical stability and mechanical, thermal and biocompatible properties [7].

3D Plastronics is a new technology allowing the integration of various electronic functions in the non-conductive polymer housing of electronic devices, by selective metallization of conductive tracks connecting surface mount devices. The polymer housing can be produced by any method known in polymer processing such as injection molding or thermoforming, but also 3D printing. The combination of 3D Plastronics with 3D printing guarantees solutions to develop prototypes for devices and systems with small dimensions. This combination offers high integration of heterogeneous electrical, mechanical, thermal and optical functions. It plays an important role in different application domains such as miniaturization of electronic devices [8], thermal management [9], medical equipment [10], automotive [11] telecommunication [12] and energy harvesting [13].

A number of techniques now exist to fully metallize non-conductive polymer surface, including SLA 3D printed parts. Among these techniques, silver painting [14,15], sputtering [16,17], conductive spray coating [18] and electroless plating [19,20]. The main issues are the adhesion of the metallic layer on the polymer surface and its electrical conductivity. These techniques generally require a preliminary surface treatment to improve the conductor-polymer interface adhesion strength, and in some case, a posterior step of copper electroplating [21] to enhance the metallic layer thickness for better electrical conductance. In this context, electroless plating, an autocatalytic chemical technique, is a metallization method of interest because, unlike the other cited techniques, it allows the full metallization of complex 3D geometry surfaces with homogeneous thickness even in inaccessible sites that are difficult to cover in depth with the other techniques [22].

One of the major challenges of the metallization of polymer surface using any of the above-mentioned methods is the metal layer adhesion on polymer. In order to promote adhesion, strong chemical oxidizing etching processes are often used to increase both surface area and wettability of the polymer surface

[23]. The most common chemical etchants used are chromic acid (CrO_3) [24], sulfuric acid (H_2SO_4) [25], potassium hydroxide (KOH) [19] and potassium permanganate ($KMnO_4$) [26] largely used in printed circuit board industry [27]. However, these products are hazardous for the environment, toxic for human and can present a serious carcinogenic risk as in the case of chromic acid [28]. Thus, there is a need to find alternatives to these chemical treatments. Literature reports the use of plasma [29] which is a safer but not very adapted method for processing complex 3D objects, besides being expensive and requiring a specific gas installation. Another method described in the literature is sandblasting which is both low-cost and within everyone's reach [30,31] and mostly used for surface preparation of substrates for metal [32] and ceramic coating [33].

Contrary to the above-mentioned processes which consist in fully metallizing the object surface for 3D Plastronics, it is necessary to selectively implement conductive tracks on the object surface in order to define an electronic circuit. Nowadays, many processes are being explored to selectively deposit conductive tracks on a 3D surface, among them: ink dispensing [12,34], wire embedding [35], two-component injection moulding (2k) [11], aerosol jet printing [36,37] and Laser Direct Structuring (LDS) [38]. LDS and 2k require specific polymers and are mostly used for Molded Interconnect Devices (MID) [39]. The majority of these techniques are very expensive because they require the use of lasers or aerodynamic systems combined with multi-axis motorized system.

This paper presents a new low-cost process, easy to implement and environment friendly, being referred to as "Rapid 3D-Plastronics". This new method combines 3D printing and 3D Plastronics for rapid prototyping of 3D plastronic devices. The fabrication strategy is based on the selective metallization by electroless copper (Cu) plating of 3D tracks produced in the form of grooves in the 3D printed surface. This method solves a major problem in 3D Plastronics since the use of complex multi-axis machining is not necessary. Another advantage is that of making conductive tracks with good electrical properties using Cu instead of conductive silver ink which has lower electrical properties (resistivity > 20 μΩ.cm). Cu adhesion was improved by modifying the surface properties using sandblasting as green process instead of sulfochromic acid or any toxic chemical agent.

In this works, first the developed process is described. Next, a detailed discussion of the characterization, capabilities and limits of the process is presented. Finally, several demonstrators for investigating high-temperature and flexible printed parts in different applications such as heating and sensing, wireless power transfer, and flexible electronic circuits are reported. The functionality of different prototypes is demonstrated as proof of concept.

2. Materials and Process

Accurate, low-cost, eco-responsible and user-friendly methods are to be selected and combined to produce 3D-parts with integrated electronic circuit. The manufacturing process can be summarized as follow: A first step consists in designing the part with integrated grooves in the surface to define the electronic tracks, and then printing it using SLA technique (Fig. 1a). The second step involves

sandblasting (Fig. 1b) to modify the wettability and the surface roughness of the polymer in order to promote the metal-polymer adhesion. A colloidal Palladium catalyst is then deposited on the entire part (Fig. 1c) and removed by hand-sanding the surface to keep the catalyst only inside the grooves (Fig. 1d). Grooves are finally metallized using Cu electroless plating (Fig. 1e) to obtain the final 3D plastronic device (Fig. 1f).

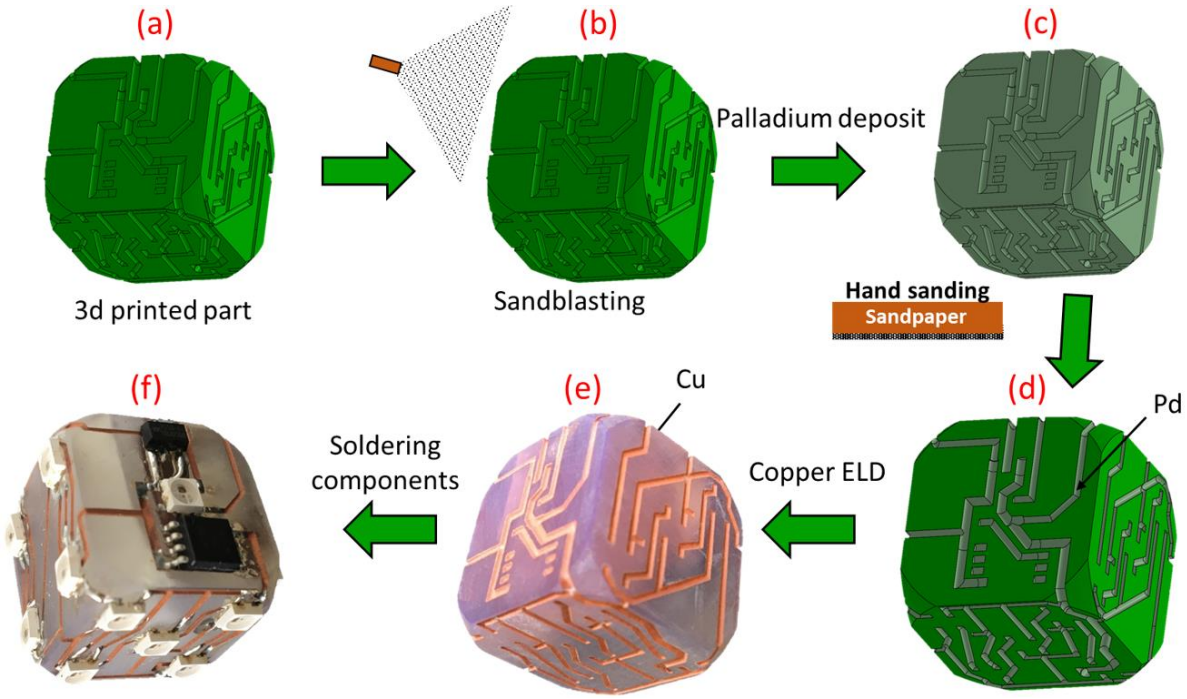

Figure 1: Process steps (a) 3D part with grooves printed using SLA technique. (b) Surface physical modification by sandblasting. (c) Colloidal Palladium deposit on the entire surface. (d) Colloidal Palladium localized only into the grooves after hand-sanding. (e) Electroless Cu plating. (f) final prototype.

2.1. Parts fabrication

A SLA 3D printer (Form 3 printer – Formlabs) was used to print all the parts to be later metallized following the developed process. This paper refers to two SLA compatible resin types based on their physical properties: i) High-temperature resin (FLHTAM-02) for its thermal characteristics, used to manufacture rigid devices for high temperature use; ii) Flexible resin (Flexible, FLFLGR02) used to fabricate 3D plastronic flexible devices. The model parts are designed using mechanical engineering CAD software. To create the electronic circuit, grooves defining the electrical tracks are added into the pattern of the 3D object surface. After 3D printing, the samples, are rinsed with isopropanol alcohol to remove resin residuals, before being thermally post-cured under UV for 60 minutes at 80°C for High temperature resin and for 15 minutes at 60°C for flexible resin to enhance their mechanical properties.

2.2. Surface treatment and Cu plating

After fabrication, the parts were then sandblasted using corundum 50 µm as abrasive. The sandblasting pressure and the working distance between the 1.2 mm nozzle and the samples were 4 bar and 5 cm respectively. Next, the samples were cleaned ultrasonically in deionized water for 10 minutes at room temperature, dried and cleaned with isopropanol, washed with deionized water. Metallization was performed by electroless plating which consists in immersing the samples in 1L of solution containing 5mL of palladium catalyst (Macuplex Activator-D34C, MacDermid) and 220 mL of 37% acid chloride (AnalaR® NORMAPUR®). The impregnation step was performed for 3 min at 30°C. After palladium catalyst deposition, the parts were rinsed with deionized water and plated for 2 h at 60°C in a commercially electroless Cu bath (Mid Copper 100XB, MacDermid). When completed, the parts were rinsed in water to remove the residual Cu electroless solution, and then air-dried at room temperature for 12h.

The Cu layer of the parts requiring a high electrical conductivity was enhanced by electroplating; the parts were plated at 30°C into a 220 g/l copper sulfate ($CuSO_4$) solution, with 3.1 % sulfuric acid (H_2SO_4), 0.2 ml/l Hydrochloric acid (HCL), and additives (0,2 ml/l Rubin T200A, 8 ml/l Rubin T200G and 2 ml/l Rubin T200E). A Cu electrode is placed at approximately 10 mm from the part. A 5 A/dm^2 current is supplied for 50 min between the electrode and the coil surface.

2.3. Characterization and Methods

2.3.1. Surface morphology

The surface morphology and the surface roughness of the 3D printed, sandblasted and metallized samples were investigated using optical microscopy (Hirox-RH-2000) and a nano point scanner NPS (NP3).

2.3.2. Contact angle

Contact angle measurements were carried out on 3D printed and sandblasted samples, using a Drop Shape Analyzer DSA30 (Kruss, Germany). The contact angle of all samples was assessed via the sessile drop technique at room temperature (23 ± 1 °C). A droplet of deionized water (9 µl) was dispensed onto the surface of the samples using a needle, and the contact angle was measured after 5s. Measurements were performed on 5 different locations of the surface of three different samples, and the average value was reported.

2.3.3. Electrical resistivity

For the electroless Cu resistivity measurement, the test specimen was a 3D printed 40 cm x 40 cm square of high temperature resin, sandblasted and totally metallized applying the same conditions as described above. The resistivity measurements were conducted at 20°C using four-point aligned Tungsten Carbide

probes with a radius of 125 µm and a pitch of 1.27 mm attached to a sourcemeter (2450 Keithley). Moreover, the thickness of the deposited Cu layer was measured using x-ray fluorescent (Bowman B series XRF). The bulk resistivity was obtained following the equation of infinite 2D sheet resistivity:

$$\rho = \frac{\pi}{\ln(2)} . \mathrm{t} . R \qquad (1)$$

Where t is the Cu thickness and R the measured resistance. A sample size correction factor of 0.990 was applied to account for the shape of the specimen. The reported values represented the average value taken from 5 different measurements collected from 5 samples.

2.3.4. Adhesion testing

To evaluate the Cu plating adhesion, first of all, a standard scotch-tape-test following the ISO 2409 test procedure was conducted on a 20 x 30 mm Cu plated surface. A sharp razor blade was used to cut a grid pattern across the sample. 2525 Scotch adhesive tape was pressed against the sample and peeled off rapidly and vertically, the percentage area moved or deformed is used to reflect the adhesion and gave the corresponding adhesion quality.

The adhesion pull-off tests were evaluated on the Cu plated surface of a sandblasted samples by a bond tester (XYZTEC Condor Sigma). Test stub with a diameter of 3 mm was glued with ethyl cyanoacrylate glue (Loctite Superglue-3) on the Cu plated surface to perform this test. An increasing tensile force is applied to the stub until coating detachment from the substrate. The fracture surface area was measured using numerical microscopy (Hirox-RH-2000, Japan). The average pull-off strength from 20 different measurements was then calculated by dividing the pull-off force by the fracture surface area.

2.3.5. Thermal and Bending tests

For heating and sensing demonstrators, thermal images were taken with an infrared thermal camera (FLIR TG267). T-type thermocouple (testo 108-2) was used to detect the temperature of the manufactured heating resistance. The resistance as function of temperature was measured using the resistance temperature detector (RTD) sensor heated up to 150°C in an oven (Memmert UF55plus).

Bending tests were carried out using an automated compression bench at a speed of 30 mm/s. The resistance of the conductor was measured 5 times with a two-point probe using a keithley (2450 SourceMeter).

2.3.6. Coils simulation and measurement

To define the design of a coil for proximity Wireless Power Transfer (WPT) described in section 3.5.3, preliminary simulations on a planar coil were carried out using the finite element magnetic method (FEMM) software [40]. Considering a coil is equivalent to a set of concentric rings, an axisymmetric 2D quasi-magnetostatic model [41,42] was chosen. Impedance and quality factor were calculated as function of frequency (1 kHz - 10 MHz) considering the skin and proximity effects. The capacitive

effect at frequencies over 1 MHz was also estimated using a coarse approach, with a simple electrostatic calculation considering the average potential of each ring. Planar coil simulation results, impedance and quality factor, were compared with experimental data obtained for a coil fabricated on a PCB, allowing us to validate our simulations. Their quality factor was calculated considering their resistivity, self-inductance and capacity using a R parallel to LC model [43].

In a second step, the model was modified for a coil on a half sphere. This allowed us to define the spiral geometry with the highest quality factor, considering the constraints due to the manufacturing process. A quality factor as high as 250 was obtained at 6.78 MHz (typical frequency used for WPT).

The impedance of the manufactured coils was measured as a function of frequency from 1 kHz up to 10 MHz using an impedance analyzer (4294A, Keysight).

3. Results and discussion

3.1. Improving Surface adhesion

The main challenge in this study was to make sure that the combination of the selected methods reflects a perfectly "compact and functional device" with properties comparable to the ones of other devices fabricated using standard processes described in literature. Therefore, a particular attention was devoted to surface preparation with sandblasting, in order to improve the surface adhesion of metal, and thereby, guarantee better electrical properties and longevity of the electronic circuit. The morphology of 3D printed sample was investigated before and after sandblasting. The parallel lines relative to the layer deposit during the 3D printing process were clearly visible on the surface of the 3D printed parts (Fig. 2a), and the surface roughness was uniform and equal to 2.38 µm (Fig. 2c). The sample had a nearly hydrophobic surface with water contact angle of 79.3° (Fig. 2e). This value is typical for stereolithography methacrylate resins [44,45]. The sandblasting treatment created micro-cavities in the surface (Fig. 2b). The surface roughness was increased evenly to 3.94 µm (Fig. 2d), and printing lines were no longer visible. The water contact angle decreases to 73.64°, indicating that the hydrophilicity of the surface of the sample had increased. The increase in surface roughness and wettability improve significantly surface adhesion [31,46].

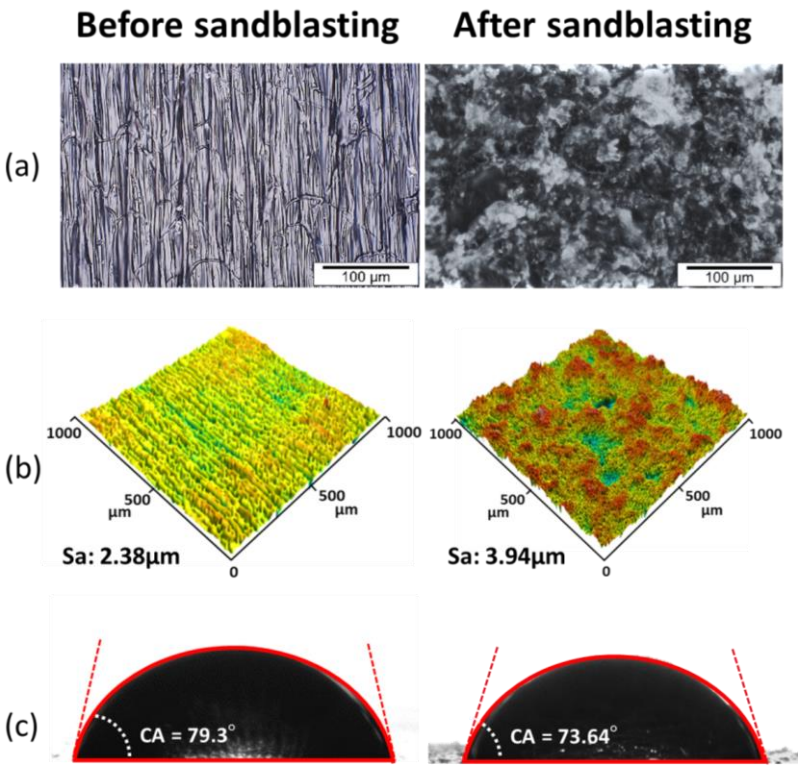

Figure 2 : 3D printed parts characteristics before and after sandblasting: (a) Optical microscope images of surface. (b) 3D presentation of surface roughness. (c) Images of water contact angle.

3.2. Selective activation of the surface

The chosen method for the activation of the surface stage did not require sophisticated equipment and that prevented the wastage of Cu. Thereby, the activation step was carried out by depositing palladium catalyst on the surface of the sample by immersion. This step was followed by surface hand sanding in order to eliminate the catalyst from all over the surface but the tracks hollowed out during printing were deeper, and thus unaffected by the surface sanding. As a result, only the grooved tracks will be metallized without any Cu waste; a considerable advantage compared to laser ablation [47] where the full surface is metallized before selectively eliminating the excess copper to keep only the electronic tracks.

3.3. Plated copper properties

After electroless Cu plating, the cross-test results confirmed the good coating adhesion on the sandblasted sample (Fig. 3b) compared to non-treated sample (Fig. 3a). Henceforth, all experimental measurements were performed on sandblasted samples. The measured pull-off strength was equal to 10.1 N/mm^2 ± 1.1.

It was noticed that the plating morphology was homogeneous and dense (Fig. 3c), and the roughness decreased down to 3.518 µm (Fig. 3d) compared to the surface roughness before plating, probably because the copper particles filled in same surface porosities hence flattening the surface therefore plating.

The electrical properties of the metallized tracks were then investigated. The measured electrical resistivity of the electroless plating Cu at 20°C was 2.25 µΩ.cm ± 0.22 for samples with a Cu thickness of 5 µm. This value corresponds to 74% of conductivity of bulk copper [48]. This resistivity remains low enough to operate a low power electronic circuit.

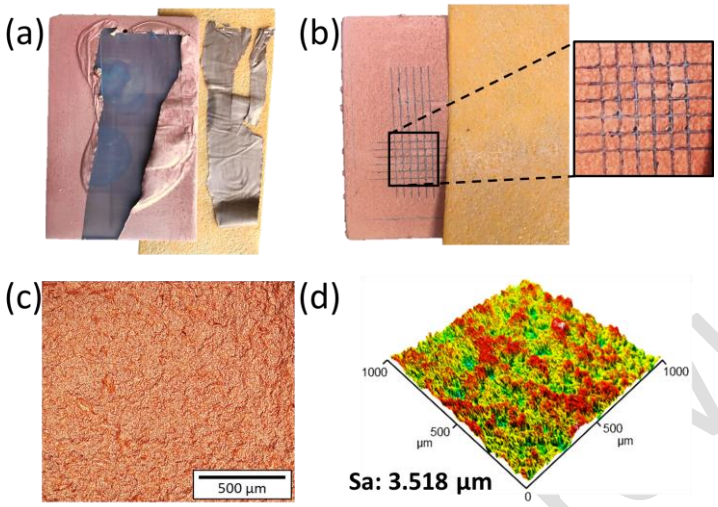

Figure 3: Electroless Cu plating samples: adhesion tape test for sample (a) without sandblasting and (b) with sandblasting. (c) optical microscopy image of Cu plating on sandblasted sample. (d) 3D presentation of surface roughness of the sandblasted Cu plated sample.

3.4. Capability and limits of the process

In order to evaluate the performance of this technique and its limits, a cube shaped vehicle test (40 mm side) with different types of tracks patterns was designed and 3D printed (Supplementary Information SI1) and treated following the process described above. Metallized tracks with widths ranging from 100 µm to 1.5 mm were studied (Fig. 4a,b). Figure 3b shows that minimum width of 200 µm enables well-defined metallized tracks with a homogeneous Cu deposit. The profile and 3D surface scanning (Fig. 4c) showed that the 200 µm width groove was still guaranteed after metallization. It was noticed that an initial depth of 100 µm has been reduced to 90 µm, due to two main reasons: (1) 3D printing, which created a rounded shape in the hollows (Fig. 4c), especially noticeable for the small dimensioned tracks (<200 µm) that approach the layer thickness; (2) the sanding of the surface, before and after the catalyst deposition, which removed a thin layer from the surface. This minimum width depends on the resolution of the 3D printer and could be further reduced for parts printed with very high-accuracy printer as microstereolithography [49]. The profile and 3D surface scanning for wider tracks for example of 500 µm (Fig. 4f) showed that the edges were well defined for a 600 µm depth.

To ensure the connection between multiple surfaces, the fabrication of vias with very high aspect ratio was investigated by adding holes into the design of the cube with diameters varying from 1 mm to 3 mm and a depth of up to 52 mm (Fig. 4a). The electrical continuity of the metallized vias was checked with a multimeter. For a diameter of 1 mm, the continuity of the via was ensured with a full hole metallization for holes up to 12 mm depth. For wider vias with a diameter of 1.5 mm, the full hole metallization can

be executed for a depth up to 36 mm. The electrical continuity was limited at 12 mm and 36 mm depths mainly due to the difficulty of the sandblasting as well as to the non-circulation of the catalyst and electroless plating solutions, what affects the homogeneity of the Cu deposit. For diameters of 2 mm and above, no electrical discontinuity was detected.

Figure 4d shows that non-planar conductive channels can be made on the same 3D printed surface, allowing the increase in the density of the circuit by exploiting the volume of the 3D part.

The metallization of spherical, square and spiral shapes has also been investigated (Fig. 4e), showing the ability of manufacturing complex shapes and patterns with this process. In supplementary information (SI2), the optical microscopy images show high magnification image of each pattern. The recommendations for the design for manufacturing (DFM) with the Rapid 3D-Plastronics are presented in supplementary information (SI3).

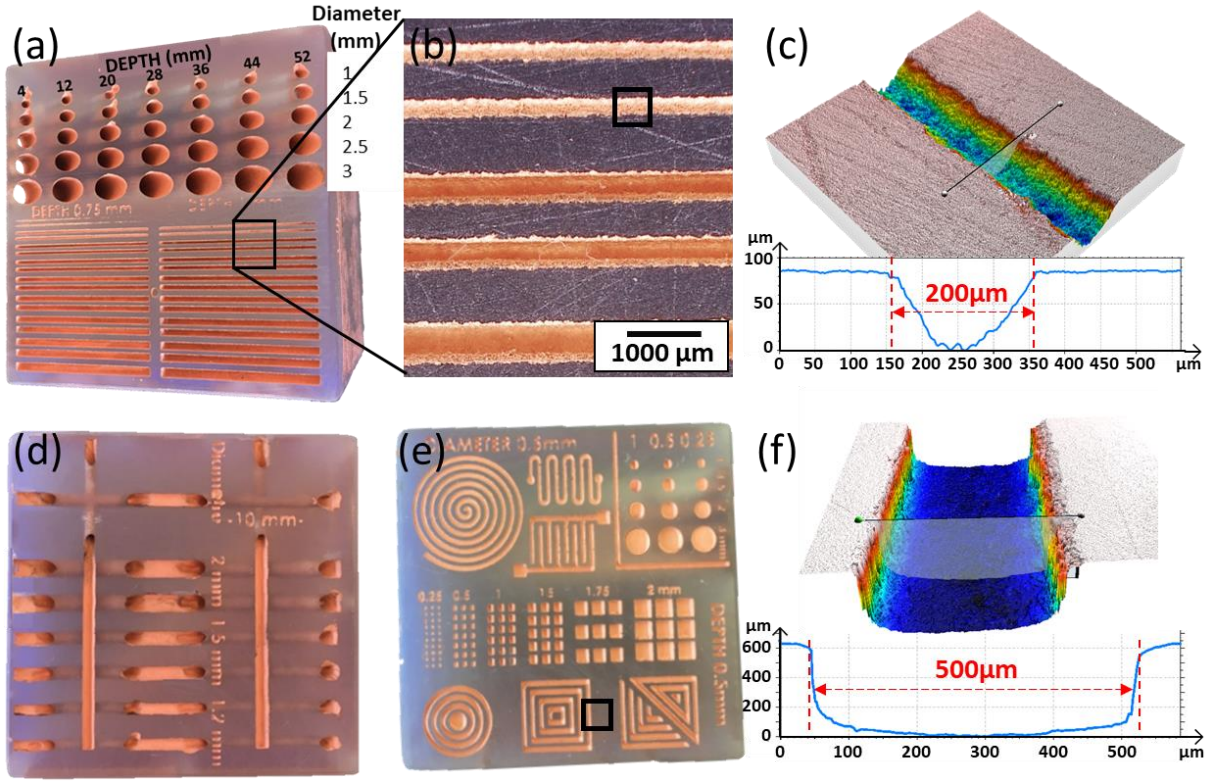

Figure 4: Cube shaped vehicle (a) metallized tracks and vias by Rapid 3D-Plastronics process, (b) optical microscopy image showing close-up of the metallized tracks, (c) profile and 3D surface scanning of the 200 µm width track framed in (b), (d) metallized channel vias, (e) metallized geometrical shape, (f) profile and 3D surface scanning of the 500 µm width track framed in (e).

3.5. Demonstrators obtained by Rapid 3D-Plastronics

3.5.1. Microcontroller based circuit

After the investigation of the feasibility and effectiveness of the developed process, its ability to make a functional plastronic device was evaluated. A 40 mm side dice shaped prototype was designed (Fig. 5a) and fabricated (Fig. 5b). The electronic circuit is based on an 8-bit microcontroller (ATtiny85),

which has the role of controlling RGB LEDs (WS2812b). The dice is powered by two CR2032 type batteries placed inside the structure. The electronic circuit and its components are described in supplementary information (SI4). The microcontroller was programmed in two modes: play mode which randomly chooses a side of the dice and turns on the corresponding LEDs when pushing the button, and demonstrator mode where the sides of the dice are turned on at random and (Fig. 5c). 3-axis accelerometer could be added to allow the microcontroller to detect the manipulated side of the dice and obtain a typical gaming dice [50].

The video 1 in supplementary information shows the dice operation in demonstrator mode. The choice was made to place the components into the 3D substrate to obtain flat facets. Vias and curvatures were used to ensure the connection between the different sides. Figure 4b shows that the manufacturing of the device by AM technology had fairly reproduced the design of the device. The components were soldered manually, and no deformation of the polymer nor Cu tracks detachment were observed, confirming the ability of soldering at high temperatures on SLA compatible resins.

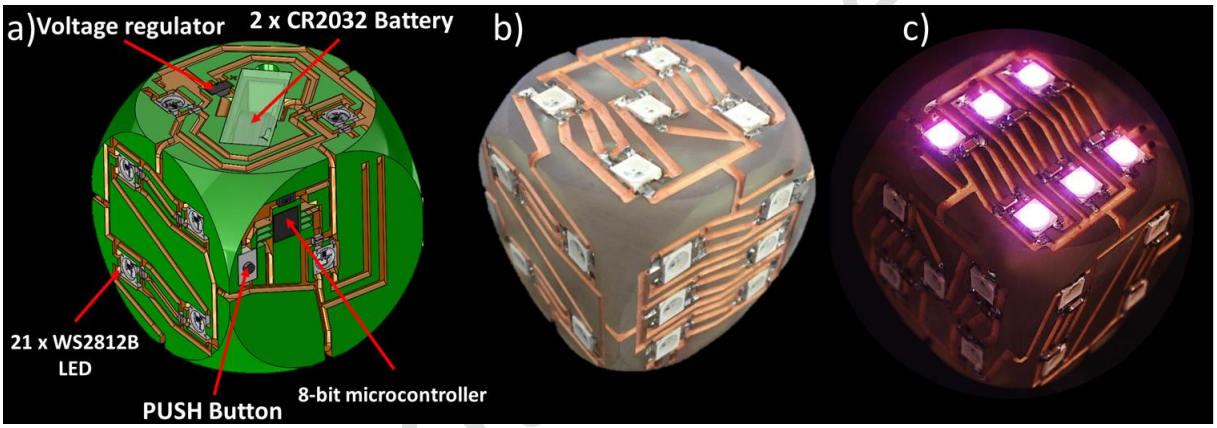

Figure 5: Gaming dice prototype: (a) electronic circuit designed into the substrate, (b) the manufactured dice after 3D printing, metallization and components soldering, (c) the functioning dice.

3.5.2. Heating and sensing

The high temperature resin has thermal properties allowing its use in high thermal conditions and was tested towards thermal applications. A heating resistance in a form of a 5 cm diameter coil was manufactured following the proposed process (Fig. 6a). The resistance was connected to a current source. The surface temperature as a function of electrical input power shows a typical curve (Fig. 6e). An electric power of 7.3 W was needed to heat the surface to 150°C. The thermal image taken at 100°C shows a homogeneous distribution of heat over the entire surface of the substrate (Fig. 6b). Moreover, the resistivity of Cu is known to change as function of temperature, which makes it an interesting material to obtain an RTD sensor [35,51]. Indeed, this idea was tested by fabricating a 3D sensor with electrodes (Fig. 6c,d) and normalized Cu resistance was measured from ambient temperature to 150°C (Fig. 6f). The linear resistance temperature coefficient (equal to 0.00327/°C) obtained between 25°C and 150°C shows that this sensor is suitable for temperature sensing.

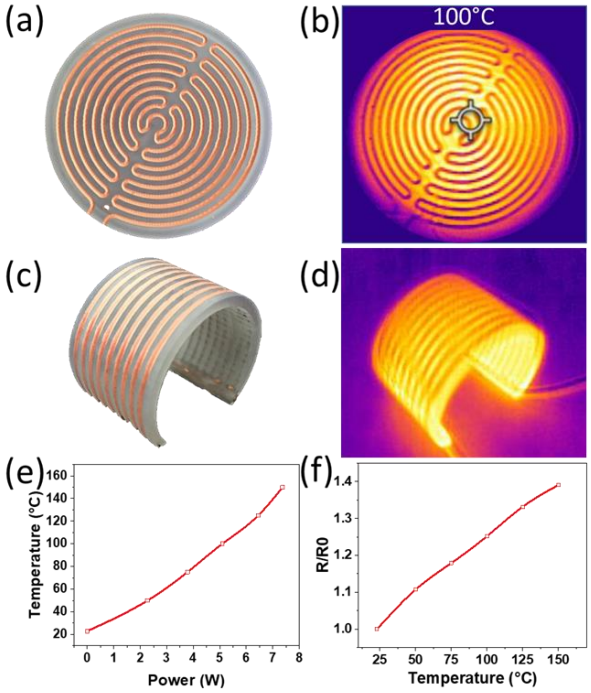

Figure 6: Heating resistance and RTD sensor: (a) picture of the fabricated 50 mm diameter heating resistance, (b) Thermal image at 100°C. (c) picture of the manufactured 3D RTD sensor, (d) thermal image of the heated RTD sensor, (e) heating resistance temperature as function of electrical input power, (f) average resistance response of RTD sensor.

3.5.3. Wireless power transfer

Another interesting application that could benefit from this process in the context of function integration is the coil fabrication on curved surface for Wireless Power Transfer (WPT). WPT was already demonstrated with plastronic devices made by LDS technology which is complex and expensive [52]. Therefore, it was interesting to use the Rapid 3D-Plastronics process to check the performance of a coil created on the curved surface of a 3D printed polymer part. In order to make a comparison with conventional manufacturing of printed board, the geometry parameters of the coil obtained by simulation using FEMM software were used to manufacture a planar spiral coil on a FR4 substrate (Fig. 7a), and a spiral coil on the surface of a 3D printed half sphere (Fig. 7b) using a 2D model (Fig. 7c) with ten turns, a track width of 950 µm and an inter-track distance of 550 µm. In the case of the FR4 substrate, the Cu thickness was 35 µm. In the case of the 3D printed part, the Cu tracks thickness initially of 5 µm made by electroless plating, was increased up to 50 µm by electrodeposition of Cu to enhance electrical conductance.

An excellent agreement between the experimental and the simulation values was noted for the impedance and also for the quality factor (Fig. 7d). At 6.78 MHz, this one was about 100 for the FR4 device and 250 for the 3D printed half sphere. The impedance values in a function of frequency are reported in supplementary information (SI5). Compared to the planar spiral coil, the spherical shape

allows to increase the self-inductance and obtain a higher quality factor due to a higher length of each turn of the coil compared to the planar shape.

The results show a better electrical conductivity and higher quality factor compared to the coils fabricated with conductive inks [53,54] allowing a better efficiency of the power transfer [55]. Moreover, the geometry of the fabricated prototype had fairly reproduced the design with high precision in opposite to a manual fabrication process used for Cu tracks [56]. Altogether, this demonstrates that the coil on a sphere is a very good candidate for WPT.

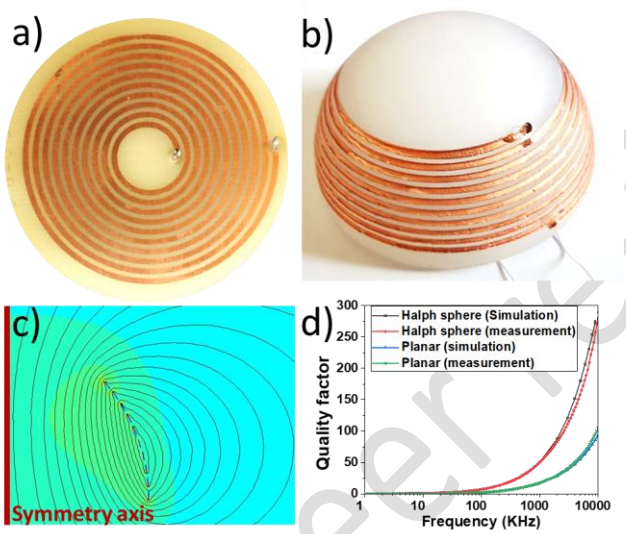

Figure 7: a) Planar spiral coil on a FR4 substrate, b) spiral coil on a 3D printed half sphere using high temperature resin, c) axisymmetric 2D model of the coil on a half sphere with the calculated field intensity distribution (A/m) using FEMM, d) Measured and simulated quality factor for the planar spiral coil on FR4 substrate and the 3D printed spiral coil using HT resin.

3.5.4. Flexible electronic circuit

SLA resins have a great range of different mechanical properties from rigid to flexible materials. Another choice of resin tested here was the flexible resin. The ability to produce flexible tracks on 3D flexible printed substrate was explored using the Rapid 3D-Plastronics process (Fig. 8a). A 3D printed substrate with straight tracks was fabricated to study the compressive behavior (Fig. 8b). The electrical normalized resistance R/R0 as a function of the number of bending cycles and bend radius was measured and reported for three samples (figure 8c-d). The resistance increase was only by 1.08 times after 50,000-cycle of bending test under 10 mm bending radius (Fig. 8c). After 20,000-cycles of bending under bend radius of 7.5 mm, the substrate undergoes cracking. The Cu tracks were then broken without having the possibility of measuring the resistance. This failure is due to the limit of the compression properties of the polymer and not of the deposited Cu. Furthermore, the Cu tracks were mechanically stable under 7.5 mm bend radius and R/R0 increased only of 6% even after 10,000 bending cycles (Fig. 8d). In addition, the Cu tracks also exhibited strong adhesion to polymer substrates, what results in high flexibility during bending, an important property for the fabrication of flexible electronic devices.

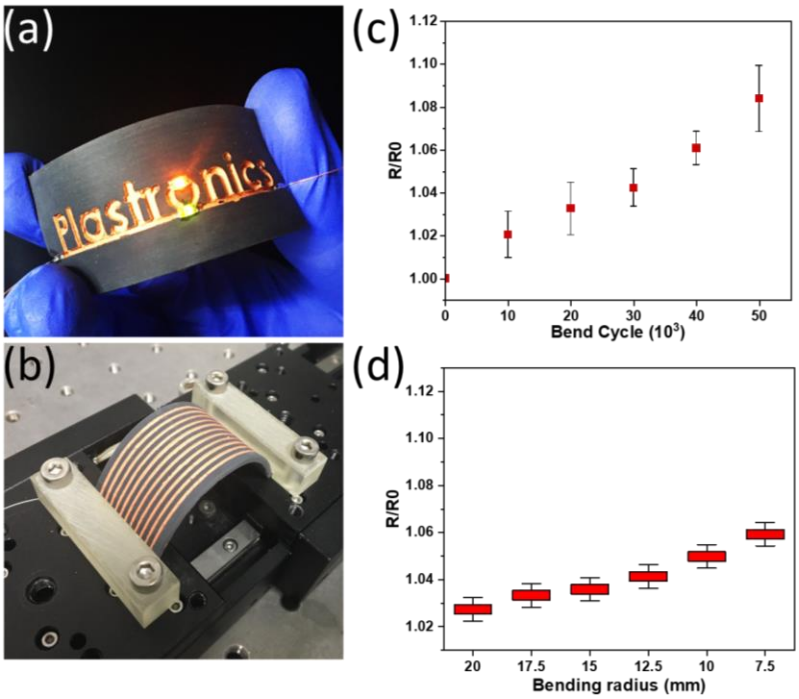

Figure 8: Flexible 3D printed electronics. (a) LEDs circuit on a 1 mm thick substrate. (b) Flexible support during bending fatigue tests (c) Bending fatigue test of Cu tracks on flexible support after 50,000-cycle of 10 mm bend radius. (d) Static bending tests of the flexible support under different bending radius.

To demonstrate the flexible device fabrication capabilities, an 8-bit microcontroller-based circuit with 3 capacitive buttons and LEDs was designed (Fig. 9a). The circuit was powered with an external 5 V power source. Figures 9b and 9c show that the circuit is operating even under bending in two different directions, which is consistent with the results obtained in bending tests. The video 2 in supplementary information shows the device in operation during bending and the operation of the capacitive buttons which have the role of changing the color of the LEDs. The success of this device paves the way for flexible plastronics prototypes.

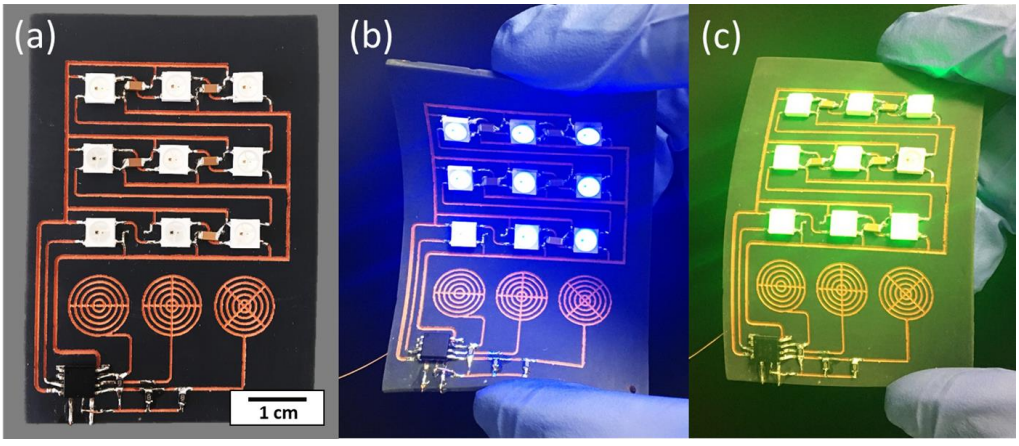

Figure 9: Flexible 3D plastronic device: (a) Photo of the device, (b,c) operating device in two bending positions.

4. Conclusion

This paper presented an original process, the “Rapid 3D-Plastronics” combining 3D printing and 3D Plastronics for rapid prototyping of highly integrated electronic devices. The use of sandblasting instead of chemical products for surface treatment before electroless plating makes this process cleaner. It also allows to reduce the contact angle and obtain a higher and regularized surface roughness, thus optimizing the Cu adhesion. Cu plated tracks with a minimum width of 100 µm and vias up to 36 mm depth were shown to be highly conductive and functional, allowing functions densification and non-planar circuit fabrication. This process has proved its ability to fabricate RTD sensors, devices that can operate at high temperature, wireless power transfer coil, flexible circuits, and 8-bit microcontroller-based circuitry.
The process is not limited to the High-Temperature and Flexible resin used in this study. The ease of manufacturing and the diversity of compatible materials offered by this process, makes it possible to obtain devices intended to operate at high temperature, chemical or biological environments. It brings an opportunity to use other resins with different properties that will be of interest for several field of applications; biomedical and mass wearable technologies. Future work is in progress to test this “Rapid 3D-Plastronics” on 3D printed high performance polymers and 3D printed ceramics intended in aeronautic and aerospace applications.

Declaration of Competing Interest

The authors declare that they have no known competing financial interests or personal relationships that could have appeared to influence the work reported in this paper.

Acknowledgements

The authors thank the French Ministry of Higher Education, Research and Innovation; the Auvergne Rhône-Alpes Region for their financial support under the PIA grant “The Plast to Be” the COMSUP program, and Ingénierie@Lyon, member of the Carnot institutes network for their financial support under the grant (MetaFab 3D project).

References

[1] T.D. Ngo, A. Kashani, G. Imbalzano, K.T.Q. Nguyen, D. Hui, Additive manufacturing (3D printing): A review of materials, methods, applications and challenges, Composites Part B: Engineering. 143 (2018) 172–196. https://doi.org/10.1016/j.compositesb.2018.02.012.

[2] E. MacDonald, R. Wicker, Multiprocess 3D printing for increasing component functionality, Science. 353 (2016). https://doi.org/10.1126/science.aaf2093.

[3] R.N. Esfahani, M.P. Shuttleworth, V. Doychinov, N.J. Wilkinson, J. Hinton, T.D.A. Jones, A. Ryspayeva, I.D. Robertson, J. Marques-hueso, M.P.Y. Desmulliez, R.A. Harris, R.W. Kay, Light based synthesis of metallic nanoparticles on surface-modified 3D printed substrates for high performance electronic systems, Additive Manufacturing. 34 (2020) 101367. https://doi.org/10.1016/j.addma.2020.101367.

[4] N. Lazarus, J.B. Tyler, J.A. Cardenas, B. Hanrahan, H. Tsang, S.S. Bedair, Direct electroless plating of conductive thermoplastics for selective metallization of 3D printed parts, Additive Manufacturing. 55 (2022) 102793. https://doi.org/10.1016/j.addma.2022.102793.

[5] M. Pagac, J. Hajnys, Q.P. Ma, L. Jancar, J. Jansa, P. Stefek, J. Mesicek, A review of vat photopolymerization technology: Materials, applications, challenges, and future trends of 3d printing, Polymers. 13 (2021) 1–20. https://doi.org/10.3390/polym13040598.
[6] A. Bagheri, J. Jin, Photopolymerization in 3D Printing, ACS Applied Polymer Materials. 1 (2019) 593–611. https://doi.org/10.1021/acsapm.8b00165.
[7] F.P.W. Melchels, J. Feijen, D.W. Grijpma, A review on stereolithography and its applications in biomedical engineering, Biomaterials. 31 (2010) 6121–6130. https://doi.org/10.1016/j.biomaterials.2010.04.050.
[8] S. Acharya, S.S. Chouhan, J. Delsing, Fabrication process for on-board geometries using a polymer composite-based selective metallization for next-generation electronics packaging, Processes. 9 (2021). https://doi.org/10.3390/pr9091634.
[9] T. Gerges, A. Marie, T. Wickramasinghe, P. Lombard, M. Leveque, S. Lips, V. Sartre, B. Allard, M. Cabrera, Investigation of 3D printed polymer-based heat dissipator for GaN transistors, in: 2021 23rd European Conference on Power Electronics and Applications (EPE'21 ECCE Europe), IEEE, 2021: p. P.1-P.9. https://doi.org/10.23919/EPE21ECCEEurope50061.2021.9570191.
[10] T. Gerges, V. Semet, P. Lombard, S. Gaillard, M. Cabrera, S.A. Lambert, 3D Plastronics for Smartly Integrated Magnetic Resonance Imaging Coils, Frontiers in Physics. 8 (2020) 1–13. https://doi.org/10.3389/fphy.2020.00240.
[11] A. Islam, H.N. Hansen, P.T. Tang, M.B. Jørgensen, S.F. Ørts, Two-component microinjection moulding for MID fabrication, in: Plastics, Rubber and Composites, 2010: pp. 300–307. https://doi.org/10.1179/174328910X12691245470356.
[12] J.J. Adams, E.B. Duoss, T.F. Malkowski, M.J. Motala, B.Y. Ahn, R.G. Nuzzo, J.T. Bernhard, J.A. Lewis, Conformal Printing of Electrically Small Antennas on Three-Dimensional Surfaces, (2011) 1335–1340. https://doi.org/10.1002/adma.201003734.
[13] X.V.L. Nguyen, T. Gerges, J.-M. Duchamp, P. Benech, J. Verdier, P. Lombard, M. Cabrera, B. Allard, 3D Plastronics Radio Frequency Energy Harvester on Stereolithography Parts, in: 2022 Wireless Power Week (WPW), IEEE, 2022: pp. 156–161. https://doi.org/10.1109/WPW54272.2022.9854010.
[14] G. Venanzoni, M. Dionigi, C. Tomassoni, D. Eleonori, R. Sorrentino, 3D printing of X band waveguide resonators and filters, 2017 32nd General Assembly and Scientific Symposium of the International Union of Radio Science, URSI GASS 2017. 2017-Janua (2017) 1–2. https://doi.org/10.23919/URSIGASS.2017.8105407.
[15] M. Dionigi, C. Tomassoni, G. Venanzoni, R. Sorrentino, Simple High-Performance Metal-Plating Procedure for Stereolithographically 3-D-Printed Waveguide Components, IEEE Microwave and Wireless Components Letters. 27 (2017) 953–955. https://doi.org/10.1109/LMWC.2017.2750090.
[16] W. Su, Z. Wu, Y. Fang, R. Bahr, P.M. Raj, R. Tummala, M.M. Tentzeris, 3D printed wearable flexible SIW and microfluidics sensors for Internet of Things and smart health applications, IEEE MTT-S International Microwave Symposium Digest. (2017) 544–547. https://doi.org/10.1109/MWSYM.2017.8058621.
[17] M.I.M. Ghazali, E. Gutierrez, J.C. Myers, A. Kaur, B. Wright, P. Chahal, Affordable 3D printed microwave antennas, Proceedings - Electronic Components and Technology Conference. 2015-July (2015) 240–246. https://doi.org/10.1109/ECTC.2015.7159599.
[18] J. Tak, D.-G. Kang, J. Choi, A lightweight waveguide horn antenna made via 3D printing and conductive spray coating, Microwave and Optical Technology Letters. 59 (2017) 727–729. https://doi.org/10.1002/mop.30374.
[19] R. Bernasconi, C. Credi, M. Tironi, M. Levi, L. Magagnin, Electroless Metallization of Stereolithographic Photocurable Resins for 3D Printing of Functional Microdevices, Journal of The Electrochemical Society. 164 (2017) B3059–B3066. https://doi.org/10.1149/2.0081705jes.
[20] J. Shen, M.W. Aiken, M. Abbasi, D.P. Parekh, X. Zhao, M.D. Dickey, D.S. Ricketts, Rapid prototyping of low loss 3D printed waveguides for millimeter-wave applications, IEEE MTT-S International Microwave Symposium Digest. (2017) 41–44. https://doi.org/10.1109/MWSYM.2017.8058593.
[21] R. Bernasconi, C. Credi, G. Natale, M. Tironi, F. Cuneo, M. Levi, L. Magagnin, Electroless Metallization of Stereolithographic Photocurable Resins for 3D Printing, ECS Transactions. 72 (2016) 9–21. https://doi.org/10.1149/07221.0009ecst.
[22] C.A. Deckert, Electroless Copper Plating A review Part I, PLATING & SURFACE FINISHING. 9 (1995) 151–159. https://doi.org/10.3109/02699059509008188.
[23] A. Holmberg, K., & Matthews, Coatings Tribology: Properties techniques and applications in surface engineering. Elsevier. Tribology Series Vol. 28, 1994.
[24] E. Sheng, I. Sutherland, D.M. Brewis, R.J. Heath, Effects of the chromic acid etching on propylene polymer surfaces, Journal of Adhesion Science and Technology. 9 (1995) 47–60.

https://doi.org/10.1163/156856195X00284.
[25] B. Luan, M. Yeung, W. Wells, X. Liu, Chemical surface preparation for metallization of stereolithography polymers, Applied Surface Science. 156 (2000) 26–38. https://doi.org/10.1016/S0169-4332(99)00339-6.
[26] Z. Wang, A. Furuya, K. Yasuda, H. Ikeda, T. Baba, M. Hagiwara, S. Toki, S. Shingubara, H. Kubota, T. Ohmi, Adhesion improvement of electroless copper to a polyimide film substrate by combining surface microroughening and imide ring cleavage, Journal of Adhesion Science and Technology. 16 (2002) 1027–1040. https://doi.org/10.1163/156856102760146147.
[27] J. LaDou, Printed circuit board industry, International Journal of Hygiene and Environmental Health. 209 (2006) 211–219. https://doi.org/10.1016/j.ijheh.2006.02.001.
[28] F. Sarto, I. Cominato, V. Bianchi, A.G. Levis, Increased incidence of chromosomal aberrations and sister chromatid exchanges in workers exposed to chromic acid (CrO 3) in electroplating factories, Carcinogenesis. 3 (1982) 1011–1016. https://doi.org/10.1093/carcin/3.9.1011.
[29] G. Rozovskis, J. Vinkevičius, J. Jačiauskiene, Plasma surface modification of polyimide for improving adhesion to electroless copper coatings, Journal of Adhesion Science and Technology. 10 (1996) 399–406. https://doi.org/10.1163/156856196X00490.
[30] M. Alonso Frank, A.R. Boccaccini, S. Virtanen, A facile and scalable method to produce superhydrophic stainless steel surface, Applied Surface Science. 311 (2014) 753–757. https://doi.org/10.1016/j.apsusc.2014.05.152.
[31] E. Njuhovic, A. Witt, M. Kempf, F. Wolff-Fabris, S. Glöde, V. Altstädt, Influence of the composite surface structure on the peel strength of metallized carbon fibre-reinforced epoxy, Surface and Coatings Technology. 232 (2013) 319–325. https://doi.org/10.1016/j.surfcoat.2013.05.025.
[32] V.P. Thompson, Sandblasting and silica-coating of dental alloys: volume loss, morphology and changes in the surface composition, Dental Materials. 9 (1993) 155–161. https://doi.org/10.1016/0109-5641(93)90113-5.
[33] L. Xu, Y. Lin, J. Li, H. Wang, J. Xu, Ka-Band Monolithic Stereolithography 3-D Printed Broadband Passive Waveguide Devices, 2018 International Conference on Microwave and Millimeter Wave Technology, ICMMT 2018 - Proceedings. (2018) 1–3. https://doi.org/10.1109/ICMMT.2018.8563939.
[34] A.J. Lopes, E. MacDonald, R.B. Wicker, Integrating stereolithography and direct print technologies for 3D structural electronics fabrication, Rapid Prototyping Journal. 18 (2012) 129–143. https://doi.org/10.1108/13552541211212113.
[35] S.-Y. Kim, J.-D. Kim, Y. Kim, H. Song, C.-Y. Park, Resistance Temperature Detector Sensor with a Copper Pattern on the Printed Circuit Board, International Journal of Control and Automation. 8 (2015) 67–74. https://doi.org/10.14257/ijca.2015.8.8.08.
[36] C. Goth, S. Putzo, J. Franke, Aerosol Jet printing on rapid prototyping materials for fine pitch electronic applications, Proceedings - Electronic Components and Technology Conference. (2011) 1211–1216. https://doi.org/10.1109/ECTC.2011.5898664.
[37] A. Mahajan, C.D. Frisbie, L.F. Francis, Optimization of aerosol jet printing for high-resolution, high-aspect ratio silver lines, ACS Applied Materials and Interfaces. 5 (2013) 4856–4864. https://doi.org/10.1021/am400606y.
[38] P. Amend, C. Pscherer, T. Rechtenwald, T. Frick, M. Schmidt, A fast and flexible method for manufacturing 3D molded interconnect devices by the use of a rapid prototyping technology, in: Physics Procedia, 2010: pp. 561–572. https://doi.org/10.1016/j.phpro.2010.08.084.
[39] J. Franke, Three-Dimensional Molded Interconnect Devices (3D-MID), Carl Hanser Verlag GmbH & Co. KG, München, 2014. https://doi.org/10.3139/9781569905524.
[40] D.C. Meeker, Finite Element Method Magnetics, Version 4.2 (21Feb2019 Build), in: 2019.
[41] E. Haddad, C. Martin, C. Joubert, B. Allard, M. Soueidan, M. Lazar, C. Buttay, B. Payet-Gervy, Modeling, fabrication, and characterization of planar inductors on YIG substrates, Advanced Materials Research. 324 (2011) 294–297. https://doi.org/10.4028/www.scientific.net/AMR.324.294.
[42] S. Zurek, FEM modelling and experimental validation of proximity loss, 4 (2017) 104–110.
[43] S. kamotesov, Transmission d'énergie par induction électromagnétique en plastronique 3D To cite this version : HAL Id : tel-02496934 Transmission d ' énergie par induction électromagnétique en plastronique 3D, Université de Lyon, 2019. Français. ⟨NNT : 2019LYSE1353⟩, p67, 2019.
[44] A.H. Hogt, D.E. Gregonis, J.D. Andrade, S.W. Kim, J. Dankert, J. Feijen, Wettability and ζ potentials of a series of methacrylate polymers and copolymers, Journal of Colloid And Interface Science. 106 (1985) 289–298. https://doi.org/10.1016/S0021-9797(85)80002-3.
[45] M. Bragaglia, V. Pascale, M. Rinaldi, F. Nanni, Silver electroless plating on 3D printed resins via stereolithography: A sustainable solution, Thin Solid Films. 757 (2022) 139417.

https://doi.org/10.1016/j.tsf.2022.139417.
[46] L. Magallón Cacho, J.J. Pérez Bueno, Y. Meas Vong, G. Stremsdoerfer, F.J. Espinoza Beltrán, J. Martínez Vega, Novel green process to modify ABS surface before its metallization: optophysic treatment, Journal of Coatings Technology and Research. 12 (2015) 313–323. https://doi.org/10.1007/s11998-014-9632-5.
[47] R. Qin, M. Hu, N. Zhang, Z. Guo, Z. Yan, J. Li, J. Liu, G. Shan, J. Yang, Flexible Fabrication of Flexible Electronics: A General Laser Ablation Strategy for Robust Large-Area Copper-Based Electronics, Advanced Electronic Materials. 5 (2019) 1–10. https://doi.org/10.1002/aelm.201900365.
[48] R.A. Matula, Electrical resistivity of copper, gold, palladium, and silver, Journal of Physical and Chemical Reference Data. 8 (1979) 1147–1298. https://doi.org/10.1063/1.555614.
[49] A. Bertsch, P. Renaud, Stereolithography, in: Three-Dimensional Microfabrication Using Two-Photon Polymerization, William Andrew Publishing, 2020: pp. 25–56. https://doi.org/10.1007/978-0-387-92904-0.
[50] E. MacDonald, R. Salas, D. Espalin, M. Perez, E. Aguilera, D. Muse, R.B. Wicker, 3D printing for the rapid prototyping of structural electronics, IEEE Access. 2 (2014) 234–242. https://doi.org/10.1109/ACCESS.2014.2311810.
[51] Z. Li, S. Khuje, A. Chivate, Y. Huang, Y. Hu, L. An, Z. Shao, J. Wang, S. Chang, S. Ren, Printable Copper Sensor Electronics for High Temperature, ACS Applied Electronic Materials. 2 (2020) 1867–1873. https://doi.org/10.1021/acsaelm.0c00358.
[52] K. Sergkei, P. Lombard, V. Semet, B. Allard, M. Moguedet, M. Cabrera, Omni-Directional Inductive Wireless Power Transfer with 3D MID inductors, in: 2019 IEEE Wireless Power Transfer Conference, WPTC 2019, IEEE, 2019: pp. 154–157. https://doi.org/10.1109/WPTC45513.2019.9055702.
[53] H. Wu, S.W. Chiang, C. Yang, Z. Lin, J. Liu, K.S. Moon, F. Kang, B. Li, C.P. Wong, B. Xu, Conformal pad-printing electrically conductive composites onto thermoplastic hemispheres: Toward sustainable fabrication of 3-cents volumetric electrically small antennas, PLoS ONE. 10 (2015) 1–11. https://doi.org/10.1371/journal.pone.0136939.
[54] T. Hou, Y. Song, W.S. Elkhuizen, J. Jiang, J.M.P. Geraedts, 3D wireless power transfer based on 3D printed electronics, in: 2018 IEEE 14th International Conference on Automation Science and Engineering (CASE), IEEE, 2018: pp. 499–505. https://doi.org/10.1109/COASE.2018.8560508.
[55] Y. Zhang, Z. Zhao, K. Chen, Frequency decrease analysis of resonant wireless power transfer, IEEE Transactions on Power Electronics. 29 (2014) 1058–1063. https://doi.org/10.1109/TPEL.2013.2277783.
[56] G.J. Gwon, Y. Kwon, Enhancement of Wireless Power Transmission Efficiency and Flexibility via an Optimized Three-Dimensional Coupled Magnetic Resonance System with Double Transmitter Coil, Journal of Electrical Engineering and Technology. 16 (2021) 1415–1426. https://doi.org/10.1007/s42835-021-00700-0.

SUPPLEMENTARY INFORMATION:

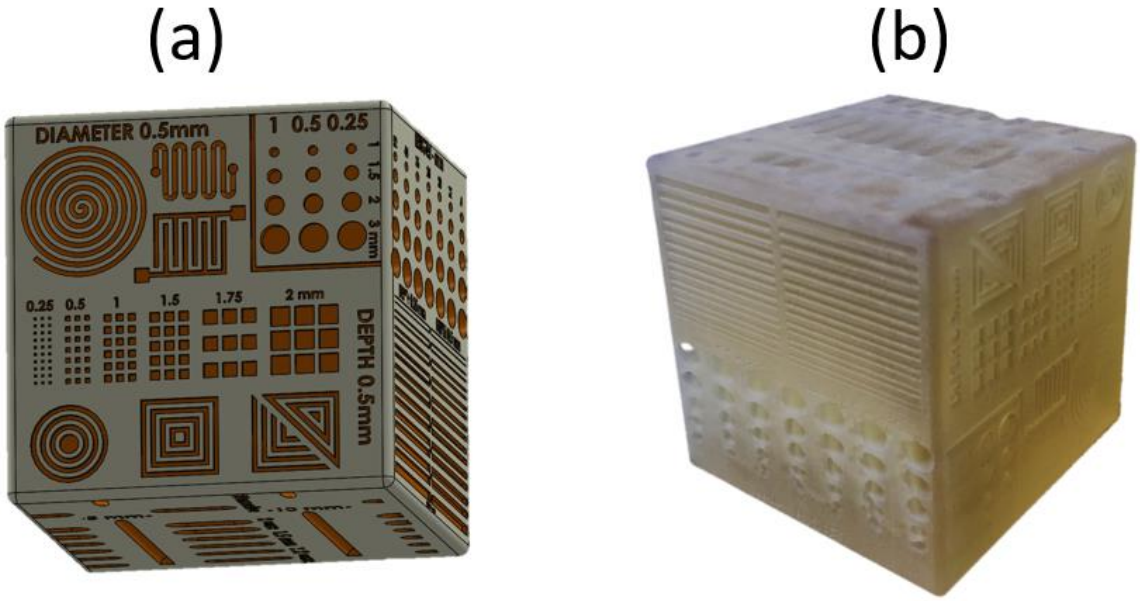

SI1: Cube shaped vehicle test: (a) CAD design and (b) 3D printed sample.

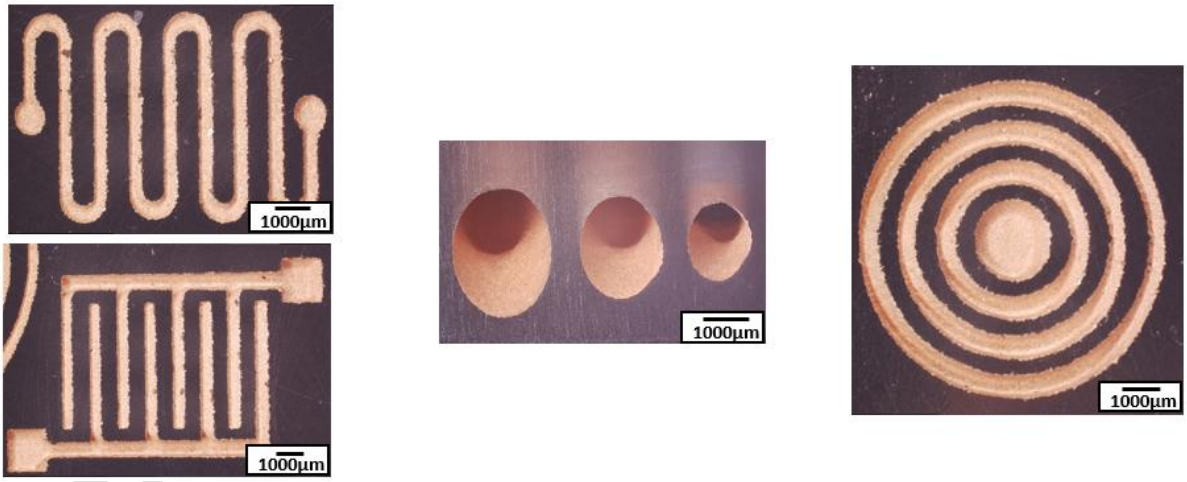

SI2: Optical microscopy images of different metallized patterns on the cube sample.

- Recommendation for traces width and spacing:

Width (w): ≥ 500 µm

Spacing (s): ≥ 500µm

Minimum trace width/spacing: 200µm/200µm

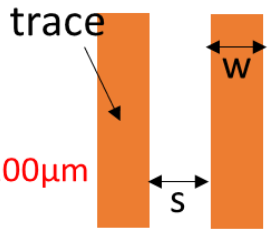

- Recommendation for via size:

Diameter (D)	Depth (d)
500 µm	500 µm
1 mm	≤ 12 mm
1.5 mm	≤ 36 mm

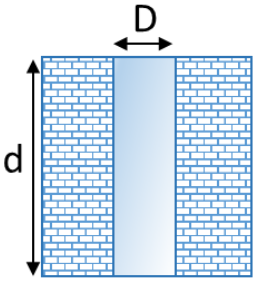

- Recommendation for traces depth and radius of curvature:

depth (d): ≥ 500 µm

Minimum trace depth: 100 µm

radius of curvature (R): ≥ 100 µm

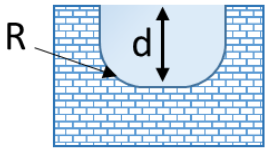

- Recommendation for Concealed channel dimensions:

Diameter (D): ≥ 1 mm

Length (L): ≤ 10 mm

Angle (θ): 30 °

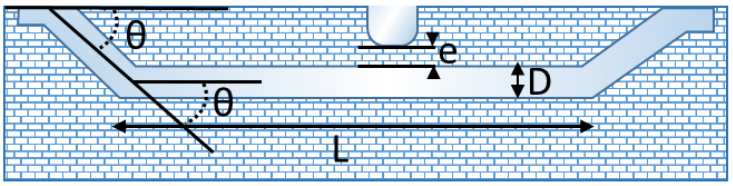

Distance between channels (e): ≥ 200 µm

SI3: Rapid 3D-Plastronics Design for Manufacturing (DFM).

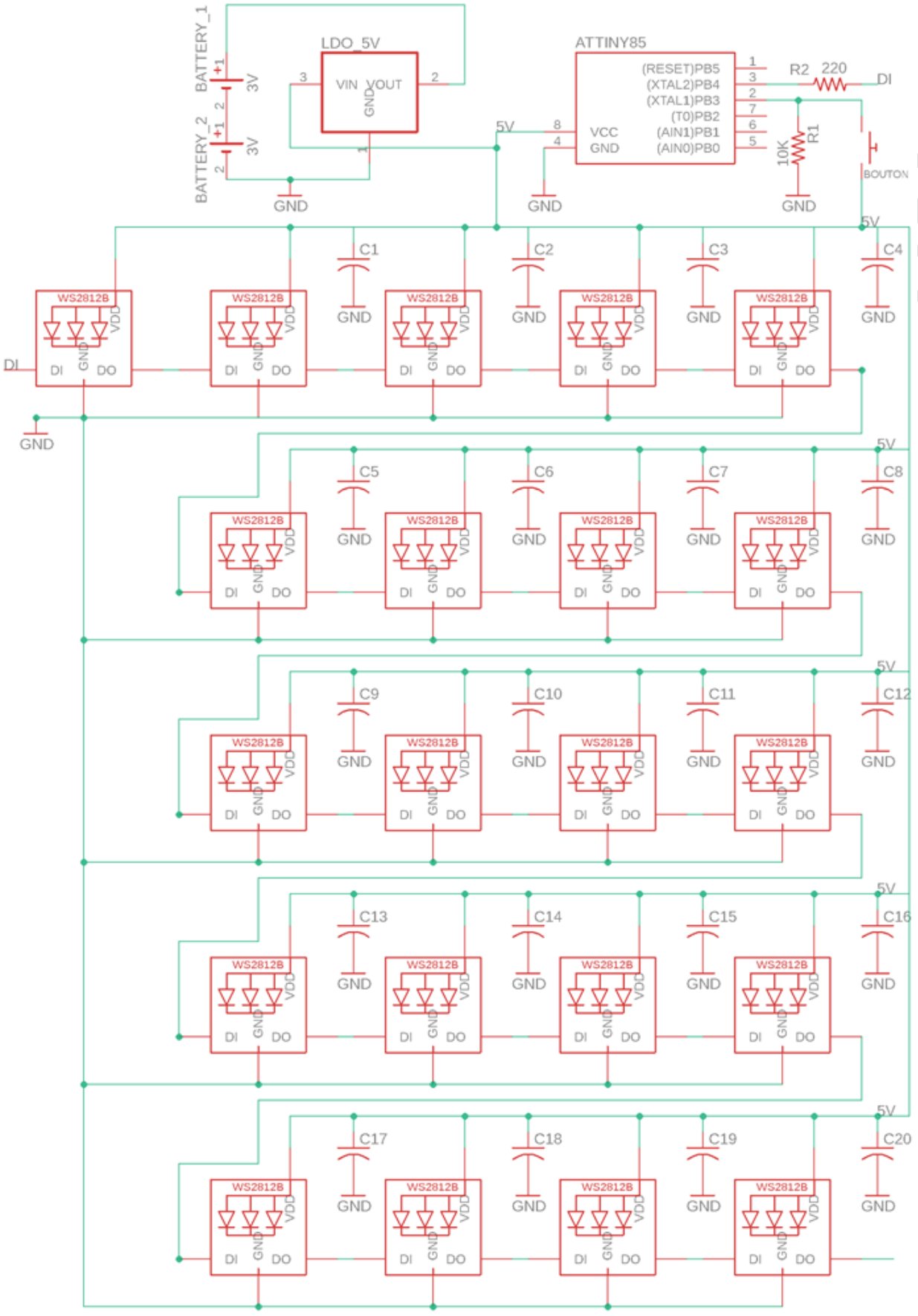

SI4: Electronic circuit designed as the gaming dice.

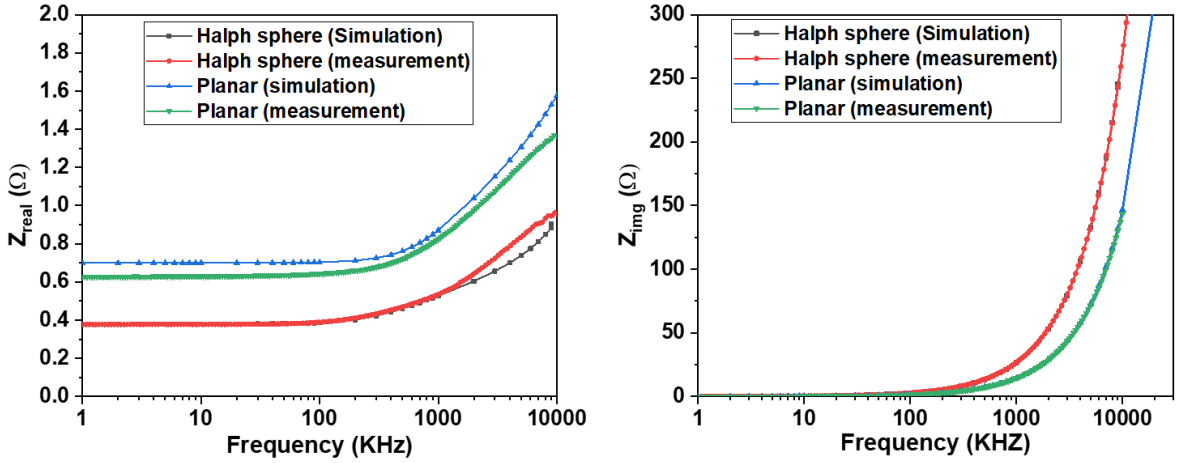

SI5: Measured and simulated planar coil on FR4 substrate and 3D printed spiral coil using HT resin: (a) Zreal and (b) Zimaginary as function of frequency.